Dispersion-to-spectrum mapping in nonlinear fibers based on optical wave-breaking

David Castelló-Lurbe,* Pedro Andrés, and Enrique Silvestre

Departament d'Òptica, Universitat de València, 46100 Burjassot, Spain

**david.castello-lurbe@uv.es*

Abstract: In this work we recognize new strategies involving optical wave-breaking for controlling the output pulse spectrum in nonlinear fibers. To this end, first we obtain a constant of motion for nonlinear pulse propagation in waveguides derived from the generalized nonlinear Schrödinger equation. In a second phase, using the above conservation law we theoretically analyze how to transfer in a simple manner the group-velocity-dispersion curve of the waveguide to the output spectral profile of pulsed light. Finally, the computation of several output spectra corroborates our proposition.

OCIS codes: (190.4370) Nonlinear optics: fibers; (190.4380) Nonlinear optics: four-wave mixing; (190.5530) Pulse propagation and temporal solitons; (060.4005) Microstructured fibers; (320.7110) Ultrafast nonlinear optics.

References and links

1. W. J. Tomlinson, R. H. Stolen, and A. M. Johnson, "Optical wave-breaking in nonlinear optical fibers," Opt. Lett. **10**, 457–459 (1985).
2. D. Anderson, M. Desaix, M. Lisak, and M. L. Quiroga-Teixeiro, "Wave breaking in nonlinear-optical fibers," J. Opt. Soc. Am. B **9**, 1358–1361 (1992).
3. G. P. Agrawal, *Nonlinear Fiber Optics*, 4th ed. (Academic, 2007).
4. D. Anderson, M. Desaix, M. Karlsson, M. Lisak, and M. L. Quiroga-Teixeiro, "Wave-breaking-free pulses in nonlinear-optical fibers," J. Opt. Soc. Am. B **10**, 1185–1190 (1993).
5. C. Finot, B. Kibler, L. Provost, and S. Wabnitz, "Beneficial impact of wave-breaking for coherent continuum formation in normally dispersive nonlinear fibers," J. Opt. Soc. Am. B **25**, 1938–1948 (2008).
6. A. M. Heidt, A. Hartung, G. W. Bosman, P. Krok, E. G. Rohwer, H. Schwoerer, and H. Bartelt, "Coherent octave spanning near-infrared and visible supercontinuum generation in all-normal dispersion photonic crystal fibers," Opt. Express **19**, 3775–3787 (2011).
7. Y. Liu, H. Tu, and S. A. Boppart, "Wave-breaking-extended fiber supercontinuum generation for high compression ratio transform-limited pulse compression," Opt. Lett. **37**, 2172–2174 (2012).
8. J. E. Rothenberg, "Femtosecond optical shocks and wave breaking in fiber propagation," J. Opt. Soc. Am. B **6**, 2392–2401 (1989).
9. V. E. Zakharov and A. B. Shabat, "Exact theory of two-dimensional self-focusing and one-dimensional self-modulation of waves in nonlinear media," Sov. Phys. JETP **34**, 62–70 (1972).
10. F. Shimizu, "Frequency broadening in liquid by a short light pulse," Phys. Rev. Lett. **19**, 1097–1100 (1967).
11. A. V. Gorbach, D. V. Skryabin, J. M. Stone, and J. C. Knight, "Four-wave mixing of solitons with radiation and quasi-nondispersive wave packets at the short-wavelength edge of a supercontinuum," Opt. Express **14**, 9854–9863 (2006).
12. L. Cohen, *Time-Frequency Analysis* (Prentice Hall, 1995).
13. R. M. Corless, G. H. Gonnet, D. E. G. Hare, D. J. Jeffrey, and D. E. Knuth, "On the Lambert W function," Adv. Comput. Math. **5**, 329–359 (1996).
14. J. Hansryd, P. A. Andrekson, M. Westlund, J. Li, and P.-O. Hedekvist, "Fiber based optical parametric amplifiers and their applications," IEEE J. Sel. Top. Quantum Electron. **8**, 506–520 (2002).

#193686 - $15.00 USD Received 10 Jul 2013; revised 2 Nov 2013; accepted 5 Nov 2013; published 13 Nov 2013

15. T. Hori, J. Takayanagi, N. Nishizawa, and T. Goto, "Flatly broadened, wideband and low noise supercontinuum generation in highly nonlinear hybrid fiber," Opt. Express **12**, 317–324 (2004).
16. J. J. Miret, E. Silvestre, and P. Andrés, "Octave-spanning ultraflat supercontinuum with soft-glass photonic crystal fibers," Opt. Express **17**, 9197–9203 (2009).

1. Introduction

Optical wave-breaking (OWB) is an effect produced by the interplay between nonlinear processes (chiefly self-phase modulation, SPM) and the chromatic dispersion of optical fibers [1]. The nonmonotonic chirp induced by SPM gives rise to the overlapping between different frequencies in the pulse tails at the normal dispersion regime [2]. This situation leads to nonlinear frequency mixing through χ^3 susceptibility. Indeed OWB can be understood in the spectral domain as a four-wave mixing (FWM) process that produces two spectral sidelobes [3]. At the same time, the interference of such frequencies results in some temporal ripples near the pulse edges.

OWB has been traditionally avoided in practice due to its inherent strong temporal fluctuations [4]. However, in the last years some works have pointed out divers benefits of this process regarding spectral broadening [5, 6] and pulse compression [7]. Particularly, we emphasize OWB as a mechanism for improving smoothness and coherence of supercontinuum spectra [6]. OWB has long been studied both experimentally and numerically [1, 8]. Nevertheless, solely the propagation distance at which the process takes place has been analytically described [2, 5], being other properties only qualitatively understood [3, 5].

In this paper, we address the study of the interaction between SPM and dispersion from a novel analytical approach based on a constant of motion conserved throughout nonlinear propagation of pulses in optical fibers. This procedure allows us to take advantage of some unexploited features related to OWB. Ultimately, we numerically identify certain situations in which we are able to transfer the group-velocity-dispersion (GVD) profile of highly nonlinear fibers to the output pulse spectrum. In principle, our derivation holds for the nonlinear propagation of pulses longer than the picosecond. However, we also discuss in heuristic terms why we expect that the physical processes behind our analysis be at least partially preserved for shorter pulses. So, we will numerically check the validity of our results spreading our simulations up to the case of femtosecond pulses.

2. Nonlinear propagation in optical fibers: a constant of motion

Spectral control of pulsed light in nonlinear fibers requires a good understanding of the interplay between dispersive and nonlinear phenomena. To this end, we tackle systems with an arbitrary dispersion profile in which SPM is the most relevant nonlinear effect. These phenomena govern ps-pulse propagation, being such evolution described by the generalized nonlinear Schrödinger equation (GNLSE) [3],

$$\frac{\partial}{\partial z}A = i\sum_{k=2}^{\infty} i^k \frac{\beta_k}{k!}\frac{\partial^k}{\partial t^k}A + i\gamma_0|A|^2A, \tag{1}$$

where A is the complex envelope of the electric field, $\beta_k = \partial^k\beta(\omega)/\partial\omega^k|_{\omega=\omega_0}$, being $\beta(\omega)$ the propagation constant of the mode supported by the waveguide and ω_0 the carrier frequency, and γ_0 represents the waveguide nonlinear coefficient. Within this framework, and without any additional assumption, in the appendix A we deduce a conservation law that generalizes a previous expression derived by Zakharov and Shabat [9],

$$\frac{d}{dz}\left(\frac{\int_{-\infty}^{\infty}\gamma_0|A(z,t)|^4\mathrm{d}t}{2\int_{-\infty}^{\infty}|A(z,t)|^2\mathrm{d}t} + \frac{\int_{-\infty}^{\infty}\beta_p(\omega)|\tilde{A}(z,\omega-\omega_0)|^2\mathrm{d}\omega}{\int_{-\infty}^{+\infty}|\tilde{A}(z,\omega-\omega_0)|^2\mathrm{d}\omega}\right) = 0, \tag{2}$$

#193686 - $15.00 USD Received 10 Jul 2013; revised 2 Nov 2013; accepted 5 Nov 2013; published 13 Nov 2013

where $\beta_p(\omega) = \beta(\omega) - \beta_0 - \beta_1(\omega - \omega_0)$ and $\tilde{A}$ is the Fourier transform of A.

In order to get physical insight into Eq. (2), on the one hand, it is worth mentioning that the nonlinear coefficient γ_0 appearing at the first fraction in the conservation law parameterizes SPM in Eq. (1). In fact, the level of significance of this nonlinear process is conventionally evaluated (assuming a nearly constant peak power of the pulse, P_0, throughout the propagation) by means of the parameter $L_{NL}^{-1} = \gamma_0 P_0$. The first fraction in Eq. (2), having also dimensions of inverse length, can be understood as a function that generalizes the classical quantity L_{NL}^{-1},

$$\mathscr{L}_{NL}^{-1}(z) = \frac{\int_{-\infty}^{\infty} \gamma_0 |A(z,t)|^4 \mathrm{d}t}{2\int_{-\infty}^{\infty} |A(z,t)|^2 \mathrm{d}t}, \tag{3}$$

and accounts for the relevance of SPM at any distance z during the propagation. At this point it is convenient to remind that the spectral broadening induced by SPM is related to the variations of the temporal intensity of the pulse [10]. Although the classical parameter L_{NL}^{-1} does not assess this pulse-profile variation, we observe that $\mathscr{L}_{NL}^{-1}(z)$ does, decreasing as the temporal pulse intensity becomes flatter and flatter.

On the other hand, if we develop $\beta_p(\omega)$ in Taylor series around ω_0, the second fraction in Eq. (2) can be rewritten as $\sum_{k=2}^{\infty} \beta_k \mu_k(z)/k!$, where μ_k is the normalized kth moment of the pulse spectrum at the baseband. This expression includes the β_k coefficients, which account for the dispersive effects in Eq. (1). For a fiber far from the zero-dispersion wavelength and assuming a smooth pulse profile during the propagation, the quantity $L_D^{-1} = \beta_2/T_0^2$ (T_0 denotes the temporal width of the input pulse) traditionally estimates the impact of dispersion. Therefore, we also define the function

$$\mathscr{L}_D^{-1}(z) = \frac{\int_{-\infty}^{\infty} \beta_p(\omega) |\tilde{A}(z, \omega - \omega_0)|^2 \mathrm{d}\omega}{\int_{-\infty}^{+\infty} |\tilde{A}(z, \omega - \omega_0)|^2 \mathrm{d}\omega}, \tag{4}$$

that generalizes the standard amount L_D^{-1}, and quantifies the action of the whole dispersive processes at the propagation distance z.

Our physical reasoning becomes particularly meaningful when Eq. (2) is rewritten as

$$\mathscr{L}_{NL}^{-1}(z) + \mathscr{L}_D^{-1}(z) = \mathscr{L}_{NL}^{-1}(0) + \mathscr{L}_D^{-1}(0) = C, \tag{5}$$

where the constant C can be calculated only taking into account the initial conditions. From this point of view, nonlinear pulse propagation can be understood as a competition between the activities of SPM and dispersion.

The above equation is going to be the key tool of our spectral control procedure in section 3. To this end, next we discuss some preliminary implications of the above conservation law under certain conditions. We emphasize that our first goal is to achieve a smooth and broad output spectrum. However, it is well-known that the spectral broadening induced by SPM is accompanied by severe spectral oscillations [10]. For this reason, $\mathscr{L}_{NL}^{-1}$ should become smaller as the pulse propagates in order to obtain a smooth output spectrum. At the same time, this requirement results in $\mathscr{L}_D^{-1}$ increases with z according to Eq. (5). Assuming that $\beta_2\mu_2/2$ is the dominant contribution in $\mathscr{L}_D^{-1}$, the above condition (i.e., $\partial_z \mathscr{L}_D^{-1} > 0$) implies $\beta_2 > 0$ since the pulse spectrum broadens through propagation along the fiber (i.e., $\partial_z \mu_2 > 0$). Therefore, as is well known, it is crucial to pump at the normal dispersion regime to achieve a smooth output spectrum in conventional fibers [5]. The above dynamics is illustrated in Fig. 1. The conditions that give rise to this evolution, namely, high nonlinearity and normal dispersion regime, become apparent in this figure through the inequalities $\mathscr{L}_{NL}^{-1}(0) \gg \mathscr{L}_D^{-1}(0)$ and $\mathscr{L}_D^{-1}(z) > 0$, respectively. It is interesting to note that, although $\mathscr{L}_{NL}^{-1}$ is the main contribution to the constant of motion at the beginning, $\mathscr{L}_D^{-1}$ dominates after a long enough z distance (say, z_{out}, the output

#193686 - $15.00 USD Received 10 Jul 2013; revised 2 Nov 2013; accepted 5 Nov 2013; published 13 Nov 2013

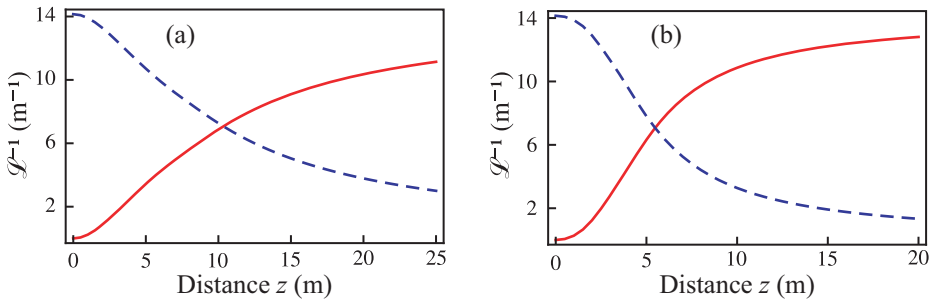

Fig. 1. Plot of the evolution of the functions $\mathscr{L}_{NL}^{-1}$ (dashed curve) and $\mathscr{L}_{D}^{-1}$ (solid curve) for a 5 ps Gaussian input pulse centered at 1550 nm ($\omega_0 = 1215\,\mathrm{rad\,ps^{-1}}$) and 100 W peak power, which propagates throughout two fibers with $\gamma_0 = 400\ \mathrm{W^{-1}km^{-1}}$ and dispersion behavior defined by: (a) $\beta_2 = 20\,\mathrm{ps^2km^{-1}}$ and $\beta_k = 0$ for $k > 2$, i.e., flat GVD profile; and (b) $\beta_2 = 20\,\mathrm{ps^2km^{-1}}$, $\beta_3 = 0$, $\beta_4 = 1\,\mathrm{ps^4km^{-1}}$, and $\beta_k = 0$ for $k > 4$, i.e., parabolic GVD profile.

distance). So, based in Eq. (5), in a first-order approximation we can write

$$\mathscr{L}_{D}^{-1}(z_{\mathrm{out}}) \approx \mathscr{L}_{NL}^{-1}(0) \approx C. \tag{6}$$

This behavior, characterized by high nonlinearity and normal dispersion, leads to a stage in which $\mathscr{L}_{D}^{-1} > \mathscr{L}_{NL}^{-1}$. In such a situation, spectral broadening cannot be mainly produced by SPM. However, as is well known, pulses that propagate at normal dispersion regime experience OWB [2]. To check that the spectral broadening in this scenario is produced by OWB, we approximately compute the distance z_c for which the new nonlinear and dispersive functions of z intersect each other. In this case we write $2\mathscr{L}_{D}^{-1}(z_c) = 2\left(\sum_{k=2}^{\infty}\beta_k\mu_k(z_c)/k!\right) = C$. As SPM is the dominant effect at the first phase of propagation, in order to calculate z_c we estimate μ_k at this distance using the SPM-induced chirp with an equivalent peak pulse power of $P_0/\sqrt{2}$ since $2\mathscr{L}_{NL}^{-1}(z_c) \approx \mathscr{L}_{NL}^{-1}(0)$ and, according to Eq. (3), the square of the power widening needs to be taken into account. If we consider a flat GVD curve, i.e., $\beta_k = 0$ for $k > 2$, and a Gaussian input pulse, we obtain $z_c \approx 1.61\sqrt{L_D L_{NL}} = 1.61\sqrt{T_0^2/\beta_2\gamma_0 P_0}$. For the case corresponding to Fig. 1(a) we get $z_c \approx 9.0$ m, which is in close agreement with the abscissa of the intersection point of the curves in this figure. In addition, the above distance is greater than the OWB distance derived in [2], $1.06\sqrt{L_D L_{NL}}$, that takes into account the point at which OWB just begins. Our conclusion is clear. We can consider z_c as the OWB distance at which OWB is the dominant nonlinear process at the second stage of the pulse propagation. Unlike the procedure for calculating the OWB distance in [2], that is restricted to certain simple cases, our interpretation allows the evaluation of z_c for both any dispersion curve and any input pulse profile. In this way, following our criterion, the OWB distance of the system corresponding to Fig. 1(b), with a non constant dispersion, turns to be $z_c = 5.5$ m.

3. Dispersion-to-spectrum mapping: direct spectral shaping through dispersion engineering

Now, if we write Eq. (6) in its integral form,

$$\int_{-\infty}^{+\infty}(\omega-\omega_0)^2\left(\frac{1}{2!}\beta_2+\frac{1}{3!}\beta_3(\omega-\omega_0)+\frac{1}{4!}\beta_4(\omega-\omega_0)^2+\ldots\right)\left|\tilde{A}(z_{\mathrm{out}},\omega-\omega_0)\right|^2\mathrm{d}\omega$$
$$\approx \frac{1}{2}\int_{-\infty}^{\infty}\gamma_0\left|A(0,t)\right|^4\mathrm{d}t, \tag{7}$$

#193686 - $15.00 USD Received 10 Jul 2013; revised 2 Nov 2013; accepted 5 Nov 2013; published 13 Nov 2013

it can be noticed that, once γ_0 and the input pulse profile are fixed, the left-hand side in Eq. (7) must go to the same value regardless of the function $\beta_p(\omega)$. It is apparent that the shape of the output pulse spectrum is strongly correlated with the waveguide dispersion during the second stage of pulse propagation ($z > z_c$), when dispersion dominates dynamics and OWB is working. With the aim of explaining this correlation, we study the spectral transfer of energy occuring during pulse propagation, focusing our attention on the power flow from red-shifted (blue-shifted) SPM-generated frequencies towards lower (higher) ones.

As we said before, OWB can be interpreted as a degenerate FWM between frequencies in the pulse tails. However, even beyond z_c we cannot ignore the nonlinear processes involving instantaneous frequencies in the central region of the pulse. In other words, the pulse evolves in the spectral domain through a set of intrapulse FWM processes [11] that involves frequencies located at both the central part and the outer tails. We use this spectral picture to study the power spreading. In order to define the waves that are nonlinearly mixed, it is convenient to write the complex envelope of the field around a generic time t_k as

$$A(t) = |A(t_k)|\, e^{i\varphi(t_k)} e^{i\left(\partial\varphi(t)/\partial t|_{t=t_k}\right)(t-t_k)}, \tag{8}$$

where we consider both a linear approximation of the phase φ and a slow variation of the envelope modulus $|A|$ compared with the phase. Equation (8) defines locally monochromatic waves with angular frequency $\delta\omega = \omega - \omega_0 = -\partial_t\varphi|_{t_k}$, power $|A(t_k)|^2$, and phase $\varphi(t_k)$. The above statement is on the basis of the physical meaning of the instantaneous frequency [12].

Next, we analyze the nonlinear pulse propagation as a process divided in the two sequential steps advanced in section 2. At the first stage, $z < z_c$, we consider that only SPM rules the pulse evolution. In this way, we can use the SPM-induced chirp to define the frequency of locally monocromatic waves at z_c. Note that the instantaneous power and frequency of every monochromatic wave can be worked out at z_c. In particular, for a Gaussian input pulse the power associated at a certain instantaneous frequency is given by

$$P(\delta\omega, z_c) = \frac{P_0}{\sqrt{2}} \exp\left[\frac{1}{2}\mathscr{W}_l\left(-\frac{1}{e}\frac{\delta\omega^2}{\delta\omega_{max}{}^2}\right)\right], \tag{9}$$

where $\mathscr{W}_l$ is the Lambert function of order l [13] ($l = -1$ for the tails and $l = 0$ for the central region of the pulse), and $\delta\omega_{\max} = \gamma_0 P_0 z_c / T_0\sqrt{e}$ is the maximum chirp achieved by the pulse at z_c [see Fig. 2].

At the second phase, $z > z_c$, each locally monochromatic wave that is present at z_c acts as the pump in multiple degenerate FWM processes with the nearby waves such that $2\omega_p = \omega_s + \omega_i$, where the subscripts p, s and i refer to pump, signal, and idler, respectively. Note that the above frequency mixing occurs at both the central part and the tails of the pulse. This panorama is graphically sketched in Fig. 2. In order to simplify the analysis, we only take into acount processes for which the pump power is much greater than the signal and idler powers ($P_p \gg P_s, P_i$) and $P_i(z_c) = 0$. In any such case, the production of idler photons for any input pulse shape is given by [14]

$$P_i(z) = P_s(z_c)\gamma_0^2 P_p^2(z_c)\frac{\sin^2(|g|z)}{|g|^2}, \tag{10}$$

where $|g|^2 = \Delta\beta\,[\Delta\beta/4 + \gamma_0 P_p(z_c)]$ is the squared modulus of the gain of a generic elementary process and $\Delta\beta = \beta(\omega_s) + \beta(\omega_i) - 2\beta(\omega_p)$ is the low power propagation mismatch. We point out that the boundary values of the pump frequencies are given by the frequencies at which the pulse chirp reaches its minimum or maximum at z_c, as one can see in Fig. 2.

Equation (10) presents a strong oscillatory behavior with z. This fact is due to the high value that the gain shows around z_c, $|g| \approx L_{NL}^{-1}$. If we average Eq. (10) along z, we obtain the trend for

#193686 - $15.00 USD Received 10 Jul 2013; revised 2 Nov 2013; accepted 5 Nov 2013; published 13 Nov 2013

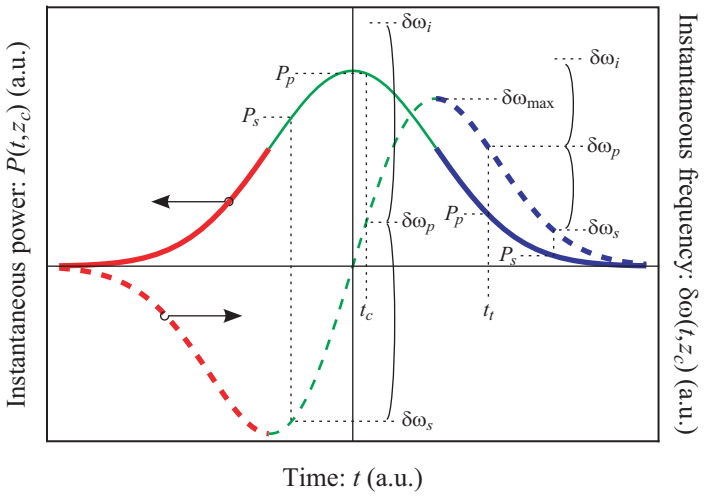

Fig. 2. Sketch for the interpretation of the FWM processes considered here. We assume that the schematic plots of the instantaneous frequency and instantaneous power correspond to the distance z_c. Thick lines denote instantaneous frequencies and their corresponding instantaneous power at the pulse tails (blue and red regions). For two cases (in the central region, t_c, and in the trailing edge, t_t), we represent an arbitrary pump wave, $\delta\omega_p$, interacting with a signal wave, $\delta\omega_s$, and producing a certain idler wave, $\delta\omega_i$.

the power corresponding to the production of idler frequencies, i.e.,

$$\langle P_i(z)\rangle \approx \frac{1}{2|g|^2} P_s(z_c)\gamma_0^2 P_p^2(z_c). \tag{11}$$

Finally the total flow from a pump frequency to the rest can be estimated by integrating for all the possible values of ω_s satisfying the above power requirements (i.e., $P_p \gg P_s, P_i$),

$$\delta P_p(z) \approx -2\int \langle P_i(z)\rangle \, \mathrm{d}\omega_s \approx -\int \frac{P_s(z_c)\gamma_0 P_p(z_c)}{\Delta\beta\left[1+\frac{\Delta\beta}{4\gamma_0 P_p(z_c)}\right]}\mathrm{d}\omega_s. \tag{12}$$

The above expression seems to diverge when $\omega_s \approx \omega_p$ since $\Delta\beta \approx 0$. However the description of those frequencies are, in fact, out of the model depicted by Eq. (10). In addition, it is easy to check, bearing in mind [14], that the net flow between two neighboring frequencies goes to zero as both frequencies approach each other. Going one step further, and according to [3], we write $\Delta\beta \approx (\omega_s - \omega_p)^2\beta_2(\omega_p)$, in the lowest-order approximation. In this way, the integrand of the right-hand side in Eq. (12), excluding $\beta_2(\omega_p)$ and $P_p(z_c)$, shows a small variation on ω_s and ω_p since it is far away from the poles. Actually, Eq. (9) can be used to verify this issue when we deal with a Gaussian input pulse. So, the above statements indicate that the power spreading rate roughly goes as the inverse of the group-velocity dispersion. This fact can be expressed in mathematical terms as

$$\delta P_p(z) \propto -P_p(z_c)/\beta_2(\omega_p). \tag{13}$$

This conclusion is in agreement with the fact that supercontinuum spectrum becomes nearly flat when $\beta_2(\omega)$ is constant [15, 16]. Note that in this case the modulus of the power flow, $|\delta P_p(z)|$, is higher in the regions in which P_p is greater. So, the power leakage shifts the spectrum power from the high values to the low ones. In this way, if z_{out} is large enough, the rapid and nearly-regular oscillations of the spectrum at the OWB distance [3] are mitigated and the output power spectrum, $S(\omega, z_{\mathrm{out}})$, becomes uniform.

#193686 - $15.00 USD Received 10 Jul 2013; revised 2 Nov 2013; accepted 5 Nov 2013; published 13 Nov 2013

When $\beta_2(\omega)$ is not constant, the above process still operates locally, in such a way that oscillations are also damped. However, the spectral power spreading is stronger when $1/\beta_2$ is larger. So, now $S(\omega, z_{\text{out}})$ should adopt the $(1/\beta_2)$-profile around the carrier frequency. At this point it is important to recognize that the variation of $-1/\beta_2(\omega)$ around the central frequency of the pulse ($\delta\omega_p = 0$) approximately agrees with that of the function $\beta_2(\omega_p)$ itself, except by a negative additive constant. This plausible conclusion is, in addition, consistent to Eq. (7) and can be mathematically expressed as

$$S(\omega, z_{\text{out}}) \sim \mathscr{M}(\omega, z_{\text{out}})\beta_2(\omega) + \mathscr{N}(\omega, z_{\text{out}}), \tag{14}$$

where $\mathscr{M}$ and $\mathscr{N}$ are in principle nearly flattened functions of ω and consequently they only account for the fine detail of the spectral shape. Despite of the approximations considered in the derivation of Eq. (14), it retains enough information about the physical processes governing the nonlinear pulse propagation and predicts a clear spectral trend within the regime where it is derived (namely, high nonlinearity and normal dispersion), as it is verified numerically in the next section.

4. Numerical results

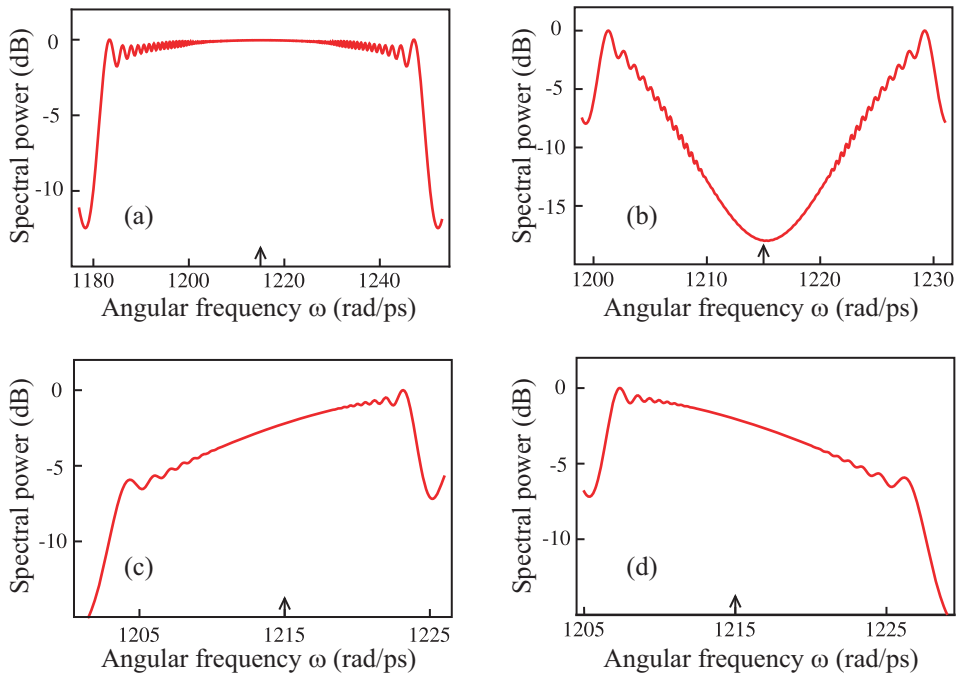

Fig. 3. Normalized output spectrum in dB for: (a) constant dispersion profile; (b) parabolic one; and linear dispersion variation with (c) $\beta_3 > 0$ and (d) $\beta_3 < 0$. See input pulse details and dispersion fiber values in the text. The small arrow corresponds to the location of the carrier frequency.

Let us consider a highly nonlinear fiber characterized by $\gamma_0 = 400\,\text{W}^{-1}\text{km}^{-1}$, and a 5 ps Gaussian input pulse with $P_0 = 100$ W, centered at 1550 nm ($\omega_0 = 1215\,\text{rad ps}^{-1}$). Our calculations include four different normal GVD-profiles. The first two cases, illustrated in Figs. 3(a) and 3(b), are that described in the caption of Fig. 1. The fiber length is $z_{\text{out}} = 25$ m in Fig. 3(a)

#193686 - $15.00 USD Received 10 Jul 2013; revised 2 Nov 2013; accepted 5 Nov 2013; published 13 Nov 2013

and $z_{\text{out}} = 20\,\text{m}$ in Fig. 3(b). The third and fourth situations correspond to linear dispersion profiles with $\beta_2 = 200\,\text{ps}^2\text{km}^{-1}$ and $\beta_3 = \pm 10\,\text{ps}^3\text{km}^{-1}$, respectively, and $z_{\text{out}} = 10\,\text{m}$. We evaluate the input pulse propagation throughout the above four fibers solving Eq. (1) by means of a Runge-Kutta-type algorithm. From Fig. 3 the conclusion is evident. Around the central ω_0-region, the output spectrum embraces the shape of the fiber $\beta_2(\omega)$-profile, in good agreement with Eq. (14). The effective spectral bandwidth covers around 90 nm in Fig. 3(a) and about 30 nm in the rest of cases. The dispersion-to-spectrum mapping is clearly achieved. It is worth noticing that the logarithmic representation of spectra mantains grosso modo the behavior described by Eq. (14) since logarithm is a soft and monotonic function.

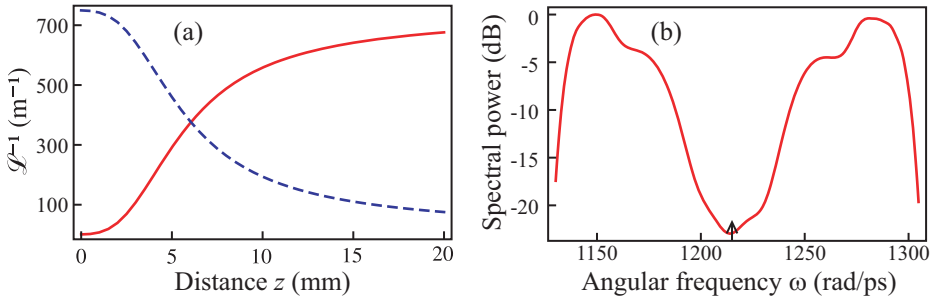

Fig. 4. (a) Plot of the evolution of the functions $\mathscr{L}_{NL}^{-1}$ (dashed curve) and $\mathscr{L}_{D}^{-1}$ (solid curve) for a FWHM 250 fs Gaussian input pulse and parabolic $\beta_2(\omega)$-fiber profile; and (b) normalized output spectrum in dB. The rest of input pulse details and dispersion fiber values are discussed in the text. The small arrow corresponds to the location of the carrier frequency.

In order to enlarge the useful spectral bandwidth, it is worth noting at this point that we achieve the above mapping by describing OWB as a combination of multiple degenerate FWM processes, provided that $\mathscr{L}_{D}^{-1}$ increases and $\mathscr{L}_{NL}^{-1}$ decreases in a smooth and monotonic way even though the sum of both quantities be not strictly constant. Based on this fact, we expect that the above mapping be at least partially preserved for femtosecond pulses. So, now we consider a 250 fs Gaussian input pulse with 5.3 kW peak power and a fiber such that $z_{\text{out}} = 20\,\text{mm}$. The rest of fiber and pulse parameters are the same as in Fig. 3(b). In this case we have included higher order effects as self-steepening and intrapulse Raman scattering in the GNLSE for the computation of the nonlinear propagation of such a pulse. The evolution of the functions $\mathscr{L}_{D}^{-1}$ and $\mathscr{L}_{NL}^{-1}$ for this situation is shown in Fig. 4(a). The resulting output parabolic spectral power shown in Fig. 4(b) confirms that we are able to achieve to a great extend the dispersion-to-spectrum mapping with ultrashort pulses. Now the useful spectral interval length is about 190 nm.

5. Conclusions

We emphasize that the new functions $\mathscr{L}_{NL}^{-1}$ and $\mathscr{L}_{D}^{-1}$ are a useful generalization of the classical parameters L_{NL}^{-1} and L_{D}^{-1} described in [3]. Going one step further, it is really notable that under certain quite usual conditions the addition of both mathematical quantities results in a constant of motion for nonlinear pulse propagation in waveguides. It is worth mentioning that their definition in terms of integrals of the pulse magnitudes leads to study the interplay between dispersion and SPM without detailed information about the pulse itself.

In the second part of the work, the above conservation law at the normal dispersion regime has been successfully applied to exploit some OWB features. Particularly, it allows to study

#193686 - $15.00 USD Received 10 Jul 2013; revised 2 Nov 2013; accepted 5 Nov 2013; published 13 Nov 2013

the OWB-induced power flow that broadens the pulse spectrum and maps the GVD shape of the fiber, $\beta_2(\omega)$, to the power spectrum profile of the output pulse, $S(\omega)$, around the carrier frequency. This result has been computationally checked even under conditions that overpass the initial input pulse requirements. We point out that this mapping permits in a very simple way to manipulate the emerging spectrum by dispersion engineering of any nonlinear waveguide in which pulse propagation is described by means of a GNLSE-type equation.

Appendix: Derivation of the conservation law

Let us write Eq. (1) in the spectral domain,

$$\frac{\partial}{\partial z}\tilde{A}(z,\omega-\omega_0) = i\beta_p(\omega)\tilde{A}(z,\omega-\omega_0) + i\gamma_0\mathscr{F}\left(|A(z,t)|^2A(z,t)\right), \tag{15}$$

where $\mathscr{F}(\circ) = \int_{-\infty}^{+\infty} \mathrm{d}t\, e^{i(\omega-\omega_0)t}\circ$. The propagation equation for the power spectrum is directly derived from the above equation,

$$\frac{\partial}{\partial z}|\tilde{A}|^2 = 2\Re\left[\tilde{A}^* i\gamma_0\mathscr{F}\left(|A|^2A\right)\right], \tag{16}$$

where $\Re$ stands for the real part of a complex expression. Multiplying by $\beta_p(\omega)$ both sides of Eq. (16) and taking into account Eq. (15), we obtain

$$\frac{\partial}{\partial z}\left(\beta_p(\omega)|\tilde{A}|^2\right) = -2\Re\left[\gamma_0\mathscr{F}\left(|A|^2A\right)\frac{\partial}{\partial z}\tilde{A}^*\right]. \tag{17}$$

At this point, if we consider $\tilde{A}^*(\omega) = \mathscr{F}\left(A^*(-t)\right)$ and apply the convolution theorem of Fourier theory, we achieve

$$\frac{\partial}{\partial z}\left(\beta_p(\omega)|\tilde{A}|^2\right) = -2\Re\left[\gamma_0\mathscr{F}\left(\int_{-\infty}^{\infty}|A(\tau)|^2A(\tau)\frac{\partial}{\partial z}A^*(t+\tau)\mathrm{d}\tau\right)\right]. \tag{18}$$

Now, integrating over ω and taking into account $\int_{-\infty}^{+\infty} e^{i(\omega-\omega_0)t}\mathrm{d}\omega = 2\pi\delta(t)$ to simplify the right-hand side, where δ is the Dirac delta function, we derive

$$\frac{\partial}{\partial z}\left(\int_{-\infty}^{\infty}\frac{1}{2\pi}\beta_p(\omega)|\tilde{A}|^2\mathrm{d}\omega + \int_{-\infty}^{\infty}\frac{\gamma_0}{2}|A|^4\mathrm{d}t\right) = 0. \tag{19}$$

Finally, Eq. (2) is obtained considering the conservation energy of these systems. Note that in the particular case $\beta_p(\omega) = (\omega-\omega_0)^2\beta_2$, we recover one of the conservation laws derived in [9].

Acknowledgments

This work was financially supported by the Plan Nacional I+D+I under the research project TEC2008-05490, Ministerio de Ciencia e Innovación (Spain), and by the Generalitat Valenciana under the grant PROMETEO 2009-077. One of the authors, D. C.-L., gratefully acknowledges funding from the Generalitat Valenciana (VALi+d predoctoral contract). P. A. and E. S. acknowledge fruitful discussions with J. J. Miret at the Universidad de Alicante, Spain.

#193686 - $15.00 USD Received 10 Jul 2013; revised 2 Nov 2013; accepted 5 Nov 2013; published 13 Nov 2013